Ana Maria Racu (Autor)

Micro-Raman spectroscopy study of ordering phenomena in YHx thin films and in CuTe2O5 single crystals

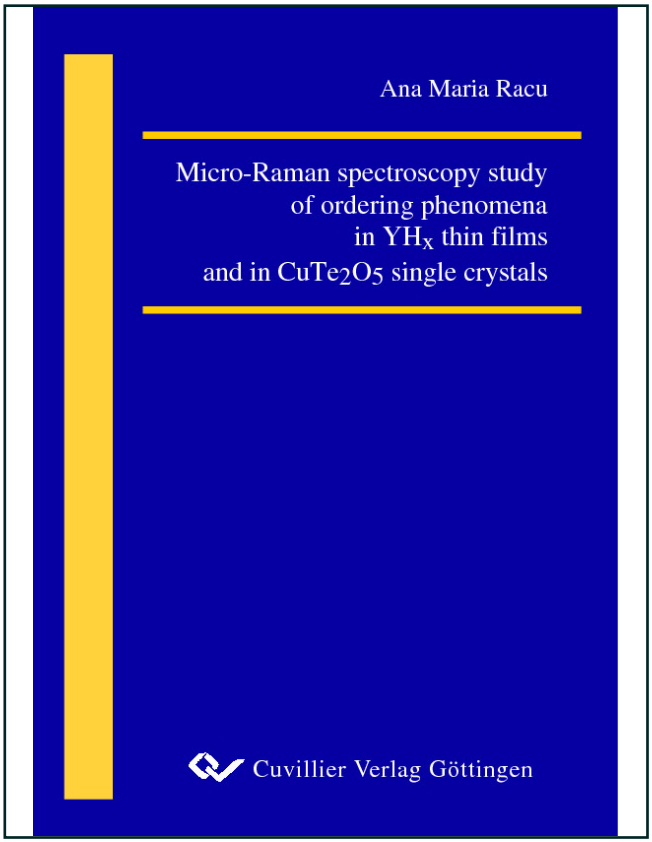

https://cuvillier.de/de/shop/publications/2480

"Hydrogen: the simplest element,
but still so versatile."

Joachim Schoenes, 2003
(Physik am Samstagmorgen)

Introduction

The physics of hydrogen in metals is exciting due to the manifold applications in technology and for basic research. Many metals absorb hydrogen when brought into a hydrogen gas atmosphere and desorb it when pumping away the hydrogen gas. The safe and compact storage of hydrogen in metals is a challenge because of the high volumetric density which can be obtained, even higher than in liquid hydrogen. The fuel cells use hydrogen as an energy carrier and produce electricity and heat whenever it is needed (Fig. 1). The metal hydrides found applications in rechargeable batteries. In these devices, hydrogen is introduced into the metal electrochemically during recharging and an electrical current flows during discharging. The rechargeable batteries are currently used in mobile applications, i. e. telephones, computers.

Hydrogen changes drastically the mechanical, electrical, magnetic and optical properties of the host metal. For example, Pd becomes superconducting and La looses its superconducting properties when loaded with hydrogen [1]. Eu and Nd change their magnetic properties from anti-ferromagnetic metals [2] to ferromagnetic semiconductors [3]. One of the most impressive transitions discovered in 1996 by Huiberts *et al.* [4] is the dramatic change in the optical properties of yttrium and lanthanum thin films near their metal-insulator transition: the dihydrides are metals while the trihydrides are insulators and transparent in the visible part of the optical spectrum. The transition from a metallic to a transparent state is reversible and occurs at room temperature simply by changing the surrounding hydrogen gas pressure or in an electrolytic cell. Soon it was shown that not only YH_x and LaH_x, but all the trivalent rare-earth hydrides and some of their alloys exhibit switchable optical properties. So far three generations of hydrogen based switchable mirrors have been discovered: (1) the rare-earth switchable mirrors, (2) the color neutral magnesium-rare-earth alloys, and (3) the magnesium-transition-metal switchable mirrors. Applications include energy-efficient windows, smart coatings in electrochromic devices, hydrogen indicators for catalytic and diffusion investigations, hydrogen sensors. A new and exciting application field is to use the switchable mirrors as hydrogen absorption detectors in a combinatorial search for new lightweight hydrogen storage materials [5]. By making thin films with controlled gradients in the local chemical composition of three or more constituents, it is possible to monitor optically the hydrogenation of typically 10^4 samples simultaneously. The goal is to find a hydrogen storage material with large hydrogen-mass and volume density and suitable absorption/desorption kinetics.

The discovery of the hydrogen based switchable mirrors challenged theoretical as well as experimental physicists to understand how the presence of hydrogen affects the electronic structure of the host metal and to investigate the origin of the metal-insulator transition in these materials. From the theoretical point of view, the problem of the phase transition is

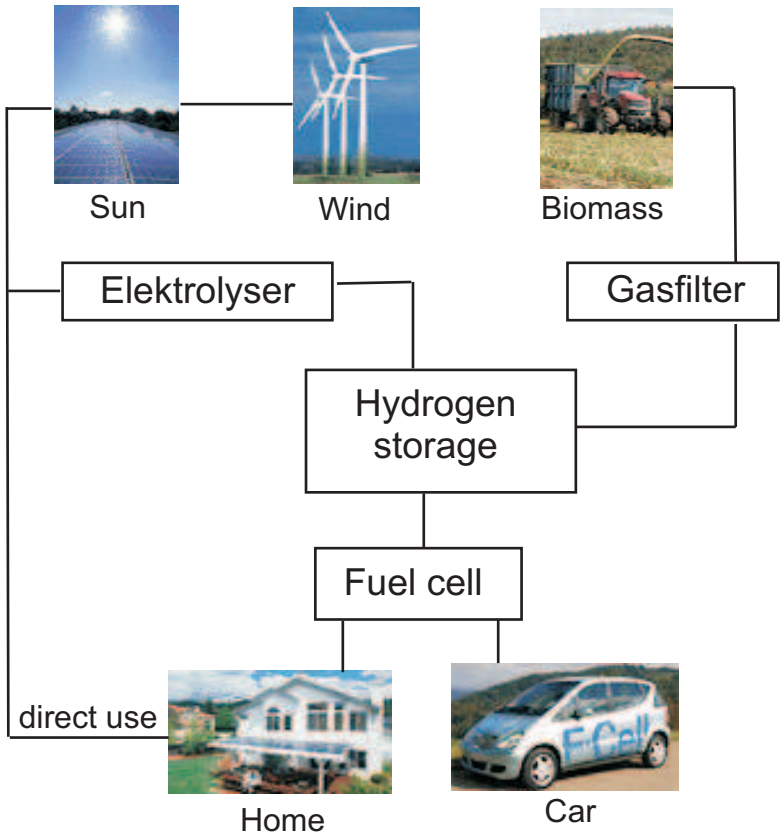

Figure 1: Fuel cells give us a very efficient way to produce electric power and heat. In the whole circle of renewable energies they are the final element. The sun provides energy, solar cells or wind power catch it, hydrogen is the storage and the medium to transport the energy and the fuel cells generate the energy whenever and wherever it is needed.

cleared in two kinds of models: broken symmetry structures and strong correlations. The latest models suppose a negatively charged hydrogen with strong correlations between the two electrons.

For the understanding of the phase transition it is important to study the structural changes and lattice distortions induced by the hydrogen in the host metal. Moreover, the only samples which retain their structural integrity during the hydrogenation are the thin films. Unfortunately, hydrogen is not accessible for x-ray diffraction experiments. On the other hand, neutron diffraction was successfully applied only for powder samples, providing information about the phonon density of states.

This thesis presents the results of a Raman spectroscopy study on the structure and the lattice distortions of metal-hydride samples. Not only the first generation switchable mirrors, i. e. rare-earth hydrides, are accessible with this method. We also present the Raman measurements on samples of the second generation switchable mirror Mg_zY_{1-z}, which we received from a collaboration with the group of Amsterdam. A complete analysis of the vibration modes and the conclusions about the structural distortions in these materials is given in Chapter 4.

Chapter 5 presents Raman measurements on single crystalline $CuTe_2O_5$ samples. Due to the low symmetry of the monoclinic structure, the calculations predict a large number of Raman modes with interesting polarization and angular intensity patterns. The number of phonons and their symmetry is calculated for the first time and compared to the Raman spectra. The observed Raman modes are identified and compared to the related compounds CuO and TeO_2. Substitutions of Zn and Ni on the Cu site preserve the crystal structure and induce changes in the magnetic properties. Moreover, a foreign phase was observed in the Raman mapping images of the sample substituted with Ni and it was identified to be TeO_2.

"We have to love nature and appreciate her wonderful gifts, her marvelous ingenuity, her resourcefulness, her infinite variety. It is the same thing that has inspired me all my life."

C. V. Raman, November 18, 1950

1 The Raman effect

When electromagnetic radiation of energy $h\nu$ irradiates a molecule, the energy may be transmitted, absorbed, or scattered. Optical spectroscopy provides numerous experimental tools to investigate optical, electronic and vibrational properties of solids. The individual techniques can be grouped into absorption, emission and scattering spectroscopies. In the Tyndall effect the radiation is scattered by particles (smoke or fog for example). In Rayleigh scattering the molecules scatter the light. Lord Rayleigh showed that the blue sky results because air molecules scatter sunlight. No change in wavelength of individual photons occurs in either Tyndall or Rayleigh scattering, i. e. they are called elastic scattering.

The effect of inelastic light scattering was discovered by Sir Chandrasekhara Venkata Raman in 1928 [6]. He was awarded the Nobel Prize in Physics 1930 "for his work on the scattering of light and for the discovery of the effect named after him". Independently, also Landsberg and Mandelstam [7] observed this effect. In the years before Raman made his discovery, inelastic scattering of light was proposed by several researchers, among them Brillouin [8], Smekal [9], and Mandelstam [10].

1.1 Inelastic light scattering

The interaction of light with a solid follows the standard laws of geometric optics and wave optics. Most experiments utilize a laser beam, which can be approximated by an electromagnetic plane wave. The processes that occur are depicted schematically in Fig. 1.1. Part of the intensity is reflected (R), whereas the remaining light enters the medium, being refracted. Inside the medium, the light is transmitted (T) and/or absorbed (A). These processes are ruled by the optical constants of the material such as the reflectivity, the refractive index or the absorption coefficient, all of which derive from the complex dielectric function. Part of the light propagating through the crystal

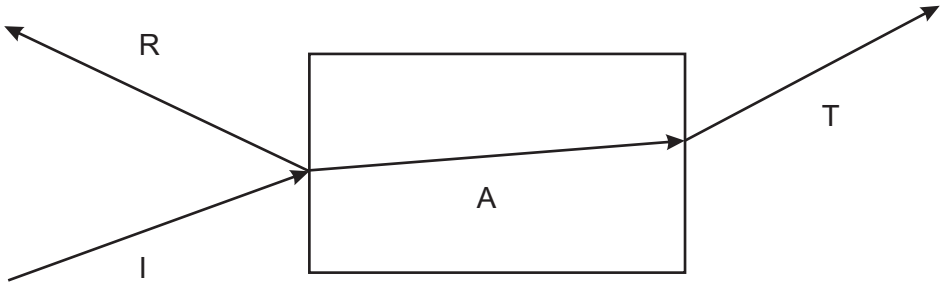

Figure 1.1: Interactions of light with a crystal. The arrows that are labelled I, R, A and T display schematically the incident light, the reflection, absorption and transmission of light intensity.

is scattered elastically (Rayleigh scattering). Only a tiny portion of the light intensity is scattered inelastically (Raman/Brillouin scattering).

Fig. 1.2 presents schematically the inelastic and elastic light scattering processes. While reflection and refraction are due to geometrical changes in the refractive index, scattering originates from inhomogeneities of the medium such as quasi-particles or defects. These inhomogeneities can be classified as being either time-dependent or time-independent, i. e. , either dynamic or static.

For purely geometrical or local inhomogeneities with no time dependence the scattering is elastic which means without a change of the light energy. The scattered intensity in the elastic processes is usually about 3 orders of magnitude smaller than the incident intensity.

Quasi-particles of the crystal can be viewed as dynamic scatterers which scatter light inelastically, accompanied by an energy transfer between light and the crystalline medium.

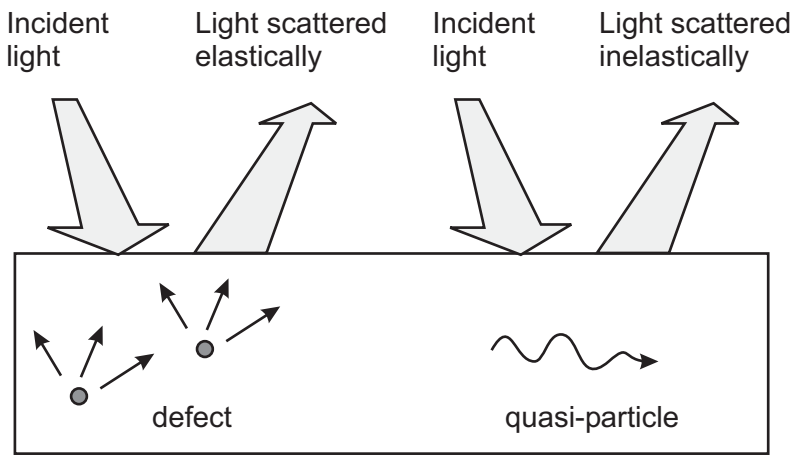

Figure 1.2: Elastic and inelastic light scattering on solids.

This is the case for the various forms of Brillouin scattering and Raman scattering on phonons. For a Brillouin or Raman spectrum, the sidebands which are equidistant from the laser frequency are typical. These sidebands are called Stokes and anti-Stokes and their associated absolute frequency difference from the laser line is called Raman shift. Accordingly, Raman spectra presented in this work are plots of the intensity of the scattered light as a function of the Raman shift, essentially a unit of energy. The inelastic scattering cross section is small, thus compared to the elastic part, reduced intensities of about 6-10 orders of magnitude are expected.

Nowadays a monochromatic and coherent laser beam is used as light source. The fact that the wavelength of the light is much larger than the interatomic distance in the crystal ($\lambda_L \gg a_0$) implies that the magnitude of its wave vector k_L is small against the typical dimensions of the Brillouin zone q_{BZ}:

$$k_L = \frac{2\pi}{\lambda_L} \approx 10^6 cm^{-1} \ll q_{BZ} = \frac{2\pi}{a_0} \approx 10^8 cm^{-1}. \tag{1.1}$$

Consequently, laser Raman spectroscopy only probes excitations near the zone center ($\mathrm{q}\approx 0$). This limitation is not given for inelastic x-ray scattering, which has recently become available at third generation synchrotrons [11]. The large wave vector of the hard x-ray radiation that is employed with this technique enables one to perform Raman experiments with meV resolution at virtually every point of the Brillouin zone. Hence, it allows for mapping out phonon dispersions, which has been traditionally achieved with inelastic neutron scattering. Unfortunately the hydrogen atoms have a very low x-ray scattering cross-section, therefore this method can not be used to determine phonon dispersion curves for the metal-hydrides thin films.

In light-scattering experiments the spectral distribution of the scattered light is analyzed relative to the spectrum of the incident light. In the case of Raman spectroscopy the changes in the spectrum are very close in energy to the energy of the incident light. The Raman shifts are of the order of a few to a few hundred wave numbers (cm^{-1}) which means a displacement of 0.1 to 10 nm. Therefore, a very good suppression of the elastically or quasi-elastically scattered light is required. Lasers are optimum as light sources of excitation while triple monochromators or notch filters are optimum for the analysis. In the experiments, four different geometries can be used as shown in Fig. 1.3.

The forward scattering and the 90° scattering are suitable only for transparent samples. For highly absorbing materials, the backscattering methods are used, where the interactions occur only close to the crystal surface [12].

1.2 Classical theory

The origin of Raman spectra can be explained by an elementary classical theory. The scattering molecule can be regarded as a collection of atoms undergoing simple harmonic vibrations. This classical approach takes no account of quantization of the vibrational energy and gives no quantitative information about the intensity of the Raman scattering.

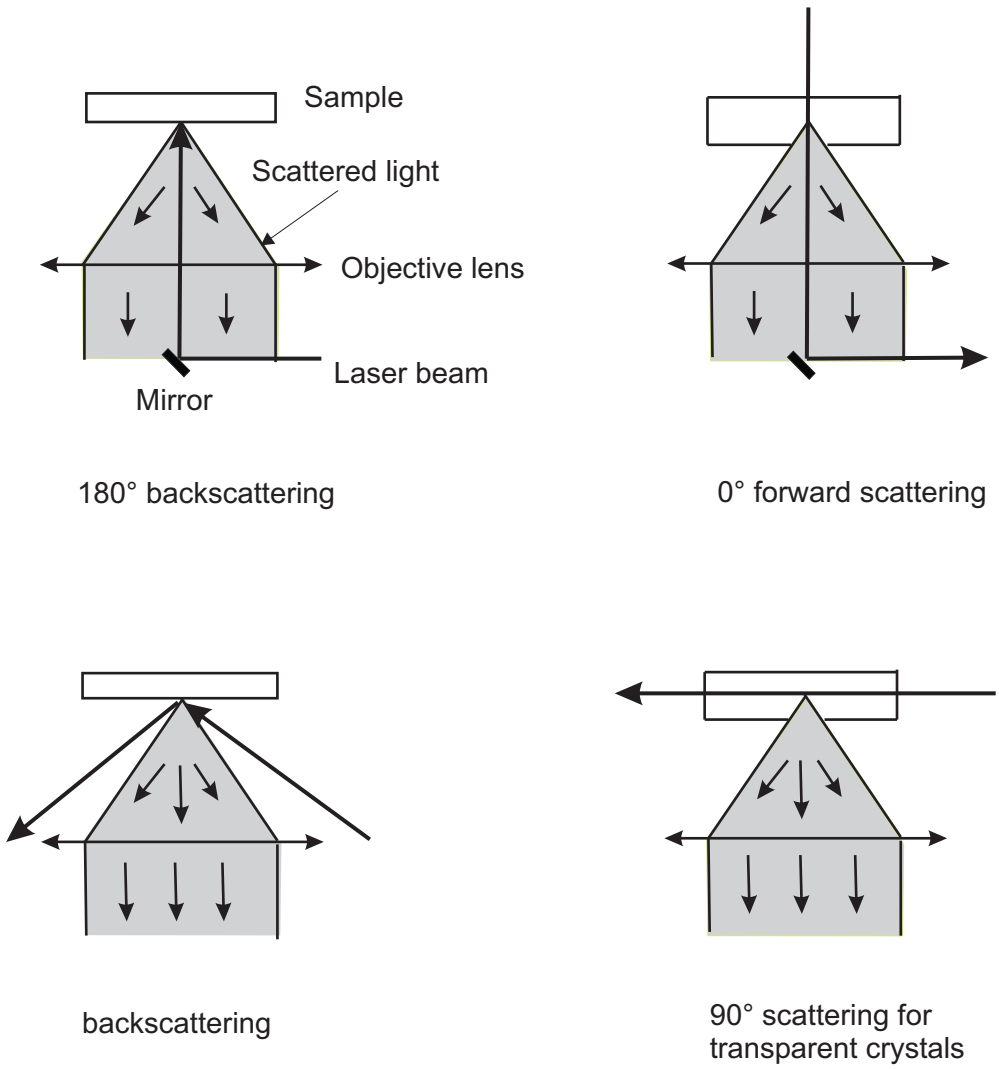

Figure 1.3: Various geometries for Raman spectroscopy experiments.

Let us consider a light wave with an electric field $\vec{E}$ and frequency ω_l which is incident on a molecule. The electric field can be written:

$$\vec{E} = \vec{E_0} \cdot \exp[i(\vec{k} \cdot \vec{r} - \omega_l t)] \tag{1.2}$$

where $\vec{E_0}$ is the amplitude and t the time. The light wave induces in a molecule a dipole moment $\vec{P}$ whose i-component is proportional to the applied field by a factor called polarizability α_{ij} and can be written as

$$P_i = \sum_j \alpha_{ij} E_j = \sum_j \alpha_{ij} E_{0j} \cdot \exp[i(\vec{k} \cdot \vec{r} - \omega_l t)]. \tag{1.3}$$

If the molecule is vibrating with frequency ν_p, the nuclear displacement $\vec{u}$ is written as

$$\vec{u} = \vec{u_0} \cdot \exp[i(\vec{q} \cdot \vec{r} - \omega_p t)] \tag{1.4}$$

where $\vec{u_0}$ is the vibrational amplitude. For small amplitudes of vibration, the polarizability α_{ij} can be expanded in a Taylor series

$$\alpha_{ij} \;=\; \alpha_{ij}^0 \;+\; \sum_k \left.\frac{\partial \alpha_{ij}}{\partial u_k}\right|_{\vec{u}=0} \cdot u_k \;+\; \sum_{k,l} \left.\frac{\partial^2 \alpha_{ij}}{\partial u_k \cdot \partial u_l}\right|_{\vec{u},\vec{u}'=0} \cdot u_k \cdot u_l \;+\; \ldots \tag{1.5}$$

where the first term denotes the electric polarizability of the medium without fluctuations and the other terms represent oscillating polarizability induced by $\vec{u}(\vec{r}, t)$. With 1.5 in 1.3 we obtain

$$\begin{aligned} P_i \;=\; & \sum_j \alpha_{ij}^0 \cdot E_j^0 \cdot \exp\left[i\left(\vec{k}\vec{r} - \omega_l t\right)\right] \;+ \\ & \sum_{j,k} \left.\frac{\partial \alpha_{ij}}{\partial u_k}\right|_{\vec{u}=0} \cdot u_k^0 \cdot E_j^0 \cdot \exp\left[i\left(\left(\vec{k} \pm \vec{q}\right)\vec{r} - \left(\omega_l \pm \omega_p\right) t\right)\right] \;+ \\ & \sum_{j,k,l} \left.\frac{\partial^2 \alpha_{ij}}{\partial u_k \partial u_l}\right|_{\vec{u},\vec{u}'=0} \cdot u_k^0 \cdot u_l^0 \cdot E_j^0 \cdot \exp\left[i\left(\left(\vec{k} \pm \vec{q} \pm \vec{q}'\right)\vec{r} - \left(\omega_l \pm \omega_p \pm \omega_{p'}\right) t\right)\right] \;+\; \ldots \\ \\ & = P_i^{(0)} + P_i^{(1)} + P_i^{(2)} \;+\; \ldots \end{aligned} \tag{1.6}$$

According to the classical theory [13], the first term describes an oscillating dipole which radiates light of frequency ν (Rayleigh scattering). The second term gives the Raman scattering of frequencies $\nu + \nu_p$ (anti-Stokes) and $\nu - \nu_p$ (Stokes). If $\partial \alpha_{ij} / \partial u_k$ is zero, the second term vanishes. Therefore, the vibration is not Raman active unless the polarizability changes during the vibration. The term $P_i^{(2)}$ gives the second order effects.
The total average power emitted by the oscillating dipole is

$$P = \frac{\omega_l^4 p_0^2}{12\pi\varepsilon_0 c^3}. \tag{1.7}$$

The emitted power and, correspondingly, the observed intensity is proportional to ω^4. For practical reasons, the frequency of the exciting laser source should be as high as possible for a good Raman signal. On the other hand if the laser frequency coincides with that of an electronic transition, resonance enhanced Raman scattering occurs. In this case the intensities of certain transitions can be many orders of magnitude larger than in normal Raman experiments. Figure 1.4 represents the mechanisms of normal and resonance Raman scattering [14].
In the normal scattering (left) the energy of the exciting line falls far below that required to excite the first electronic transition and the frequency of the laser has no influence on